

Article

Structural Dynamic Model Updating with Automatic Mode Identification Using Particle Swarm Optimization

Kaiyang Li ¹ , Jie Fang ^{1,*}, Bing Sun ¹, Yi Li ² and Guobiao Cai ¹¹ School of Astronautics, Beihang University, Beijing 100191, China² Beijing Institute of Spacecraft Environment Engineering, Beijing 100094, China

* Correspondence: mdorg@buaa.edu.cn

Abstract: Dynamic model-updating methods are a useful tool for obtaining high-precision finite element (FE) models. However, when using such methods to update a model, there will be problems with incompleteness and mode switching. To overcome these problems, this paper proposes a structural dynamic model-updating with an automatic mode-identification method. In this method, a mode-identification index is established based on image-similarity recognition to identify the consistency between FE and experimental mode shapes, and particle swarm optimization is introduced to update the model. In addition, to reduce the computational time, Latin hypercube sampling is employed to perform probability statistics of the switching range of the concerned mode orders, and the orders of mode identification are reduced according to the statistics results. In this paper, the proposed method was validated by model-updating of a square plate. The natural frequencies and mode shapes of the plate were obtained by experimental modal analysis and used as the updating objectives of the FE model. In addition, the boundary condition of the plate was simplified by a series of springs, which were used as updating parameters along with material properties and dimensions. Finally, the FE model of the plate was updated by the present method, and the results indicate that the objective function of the updated FE model was successfully reduced from 14.31% to 1.05%, which proves that the proposed model-updating method is effective and feasible.

Keywords: dynamic model-updating; mode switching; mode identification; particle swarm optimization; modal analysis



Citation: Li, K.; Fang, J.; Sun, B.; Li, Y.; Cai, G. Structural Dynamic Model Updating with Automatic Mode Identification Using Particle Swarm Optimization. *Appl. Sci.* **2022**, *12*, 8958. <https://doi.org/10.3390/app12188958>

Academic Editor: Giuseppe Lacidogna

Received: 18 July 2022

Accepted: 31 August 2022

Published: 6 September 2022

Publisher's Note: MDPI stays neutral with regard to jurisdictional claims in published maps and institutional affiliations.



Copyright: © 2022 by the authors. Licensee MDPI, Basel, Switzerland. This article is an open access article distributed under the terms and conditions of the Creative Commons Attribution (CC BY) license (<https://creativecommons.org/licenses/by/4.0/>).

1. Introduction

In structural dynamic engineering, the development of reasonable finite element (FE) models can guarantee the reliability of structural analysis. Nevertheless, discrepancies always exist between measured and FE model predicted behaviors, which can be due to uncertain structure properties, model simplification, and/or inappropriate boundary conditions [1]. Therefore, to reduce these discrepancies, it is often required to update the FE model based on measured data. The dynamic model-updating method is an important means of building a high-precision FE model, which can reflect the dynamic characteristics of the actual structure.

In general, dynamic model-updating methods can be classified into matrix updating methods, also called direct updating methods [2–4], and parameter updating methods, also called iterative updating methods [5–7]. In matrix updating methods, the mass, stiffness, and damping matrices of the FE model are directly updated to generate an accurate model by one-step procedure calculation, which is a very efficient approach. However, the matrices of the updated model lose the symmetry and sparsity of the original matrices, leading to lack of physical significance [4]. Thus, in practice, it is difficult to use these methods to provide clear guidance. In contrast, parameter updating methods update the FE model by adjusting physical parameters, such as material parameters, geometric dimensions, and connection and support stiffness characteristics, which are much closer to physically

realizable quantities [5]. Compared to matrix updating methods, parameter updating methods are more acceptable and have been widely used in structural engineering. In a sense, the model-updating process using the parameter updating method can be regarded as an optimization problem, since model-updating is essentially an inverse problem, where a deterministic objective function is adopted to obtain the precise FE model by seeking the optimal structural parameters [8]. Consequently, in parameter updating methods, a reasonable optimization model and an efficient optimization algorithm are the key elements to obtaining an accurate FE model.

It is common knowledge that the development of an optimization model generally includes three factors: design variables, objective functions, and constraints. In model-updating, the primary issue concerns the construction of the objective function, which aims to quantify the discrepancies between the actual structure and the corresponding FE model. Frequency response functions (FRFs) [9–12] and modal parameters, such as natural frequencies and mode shapes [13–15], are commonly used to form the objective function. FRF data of the actual structure obtained from vibration tests can be directly applied in model-updating. The FRF-based model-updating method was first proposed by Lin and Ewins [16,17], who successfully applied it to update undamped structure models. Subsequently, this method was further extended by Lin [9] to update linear damping models. Since then, FRF-based model-updating methods have been further developed. However, measurements of FRF data are susceptible to environmental noise, which may lead to inaccurate model-updating. Moreover, in practice, FRF data are usually inaccessible, since the excitation loads of engineering structures are often difficult to determine. Such deficiencies hinder the wide application of the FRF-based model-updating method in practical engineering. On the other hand, modal parameters can be easily extracted from the response data of a structure using modal-analysis techniques under operational conditions. In addition, compared to the FRF-based model-updating method, the natural frequency- or mode- shape-based model-updating method uses only few residual discrete frequencies of interest, thus avoiding the unnecessary time consumption induced by the use of uninteresting frequency data over the entire frequency domain.

Nevertheless, model parameter-based model-updating methods are associated with certain problems that need to be tackled. Modal pairs, including natural frequencies and mode shapes, are the most commonly used modal parameters in model-updating, and can be used separately or combined. The natural frequency is the overall attribute of a structure and can be accurately identified from the response data either in the time or frequency domain. In model-updating, the absolute or relative errors of experimental and analytical natural frequencies can be used directly as the objective function [13]. The mode shape is the local attribute of a structure; that is, theoretically, the measurement of complete mode shapes requires countless measuring points, which cannot be realized experimentally. Therefore, an incompleteness problem in measurement data inevitably exists in this type of method since the obtained data contain fewer modes than the order of the identified numerical model [1]. As a result, the modal order measured from the actual structure does not correspond to the numerical model. Furthermore, mode switching mostly occurs in the model-updating process, since not every mode can be changed within the same step [18]. In other words, the sensitivity of each order mode to the structural parameters is different. After multiple iteration steps, the change of adjacent modes could be greater than the difference between them, resulting in mode switching. If mode switching is not taken into consideration, it is likely to disturb the model-updating process and result in an ill-conditioned updated model.

In order to overcome the aforementioned problems, it is necessary to assess the consistency between experimental and analytical modes. Compared to the natural frequency of a structure, its mode shape contains rich modal information. Therefore, in the literature, many studies have taken the mode-shape information of the structure as the main criterion to measure the consistency between modes. The modal assurance criterion (MAC) proposed by Allemang [19], and its derivatives, can effectively solve this problem, and due

to their simple statistical concept, they have become the most widely used quantitative indicators [18]. Guo [13] introduced the coordinate strain modal assurance criterion (COS-MAC) to quantify the difference between experimental and numerical strain mode shapes, and combined the error of natural frequencies to construct an objective function for model-updating. In their study, the quantified results of the consistency between experimental and analytical mode shapes were taken as the target for correction, and the optimal value was obtained if and only if the experimental and numerical modes were of the same order mode. Li [5] proposed an improved MAC to assess the similarity of mode shapes. In the model-updating process, the improved MAC was applied to identify the analytical modes that match the measured modes to ensure the accuracy of the updated numerical model. According to the above studies, the MAC is an effective index to identify or track modes; however, it is not sensitive to mode-shape changes, since all mode-shape differences are considered in the scalar of a single global index [20]. In the sparse mode region in the frequency domain, the similarity of mode shapes in a relatively wide frequency range near each order mode is high. For example, if the frequency was taken as the objective, it would inevitably lead to a large model-updating error. In this paper, inspired by the image recognition technology, a mode-identification index based on image-similarity recognition (ISR) is proposed to provide a novel approach for mode identification.

Model-updating of complex structures may involve hundreds of design variables, which limits the extensive use of traditional gradient optimization methods, since the quantitative relationship between the design variables and the objective function is difficult to be described mathematically. To overcome such problems, the application of intelligent optimization algorithms has received extensive attention in recent years. Inspired by the observation of birds flocking and searching for food, Eberchart and Kennedy [21] proposed particle swarm optimization (PSO), which is a representative intelligent optimization algorithm. PSO is a global optimization algorithm that can simultaneously search for the optimal value in the entire design domain and does not rely on gradient information; thus, it has the characteristics of easy operation and fast convergence. Consequently, this study proposes a structural dynamic model-updating method with automatic mode identification using PSO.

The paper is organized as follows: In Section 2, the experimental and FE modal-analysis results are presented and discussed. In Section 3, a new mode-identification index (ISR) is introduced and the structural dynamic model-updating method with automatic mode identification using PSO is described in detail. In Section 4, the optimization model is established, and the optimal results are discussed in Section 5. Finally, the conclusions are drawn in Section 6.

2. Experimental and Finite Element Modal Analysis

To prove the feasibility and effectiveness of the method proposed in this study, a square plate was selected as the model-updating object. In this section, we describe how the square plate, where the natural frequencies and mode shapes were obtained, was manufactured for vibration tests. Subsequently, based on the initial design parameters, a parameterized FE model of the plate was developed, and an FE modal-analysis test was performed. In the final part of this section, we discuss the errors between the experimental and numerical results.

2.1. Experimental Modal Analysis

Modal-analysis tests usually require an excitation system, a measurement system, and a data-analysis system. In this study, the experimental modal analysis was performed by means of a sinusoidal sweep, and a schematic diagram of the entire experimental modal-analysis system is illustrated in Figure 1. In the test, a vibration exciter (YMC L-800 type) was used to generate the exciting force for the plate, which was fixed to the exciter with a bolt (Figure 2). An eight-channel acquisition analyzer (m + p VibPilot) and a personal computer were used to perform the data analysis.

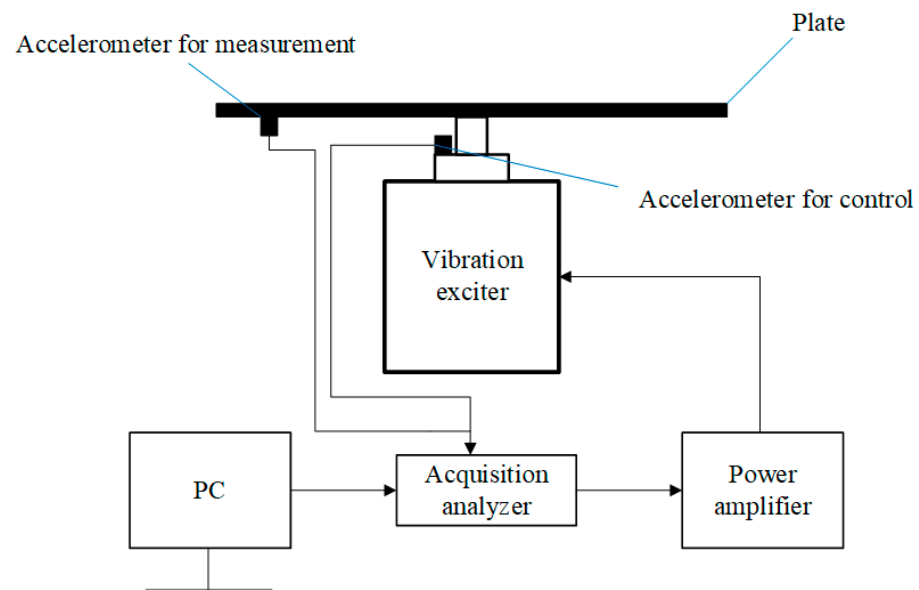


Figure 1. Schematic diagram of the experimental modal-analysis system.

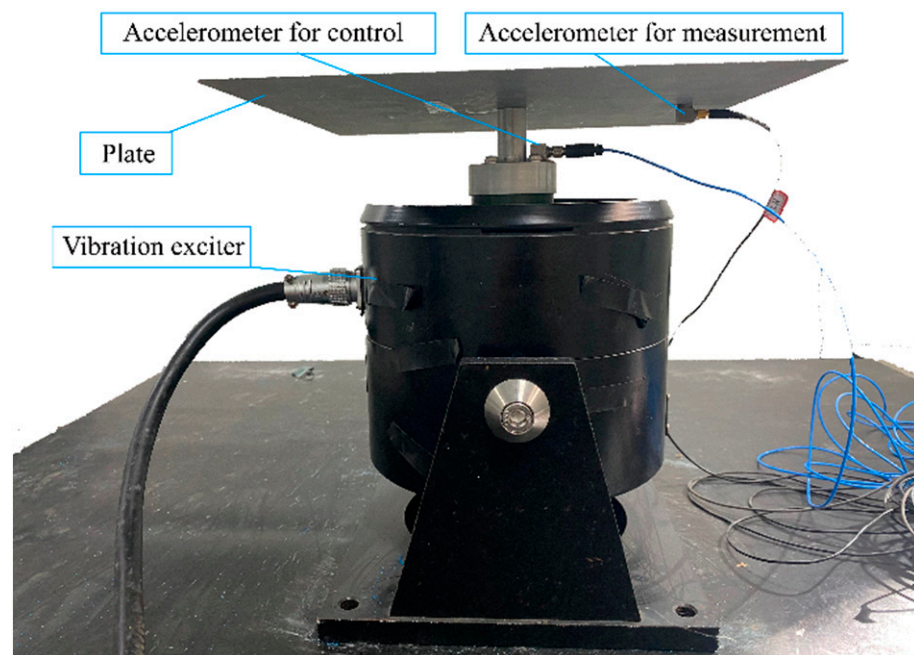


Figure 2. Experimental configuration: The plate and the vibration exciter.

To measure the natural frequencies and mode shapes of the plate, a novel measurement system was designed. More specifically, two accelerometers, one for control and the other for measurement, were used to acquire the frequency response data. Compared to the measurement of the natural frequency, it is relatively difficult to measure the mode shape of the structure, since the mode-shape data are different for different locations. To this end, there are some useful techniques based on high-precision laser instruments, which can obtain almost complete mode shapes in a contactless way [22,23]. Nevertheless, most of these techniques are expensive and inoperable. In order to measure full-field mode shapes in a simple and affordable way, a fine-sand vibration method was employed in this study. During test operation, fine colored sand was uniformly spread on the top of the plate (Figure 3), and when the plate resonated, the corresponding mode shape could be observed on the plate.



Figure 3. Fine colored sand spread on the plate.

The test conditions used in the experimental modal analysis are listed in Table 1, and the test procedure comprised the following steps:

Table 1. Frequency sweep test conditions.

Test Type	Sweep Frequency Range	Excitation Value	Sweep Time
Broadband frequency sweep test	200 Hz~1500 Hz	0.1 g	5 min
Narrow-band slow frequency sweep test	Within $\pm 5\%$ of the natural frequency	2 g	3 min

Step 1. Perform a broadband frequency sweep test to obtain the frequency response data of the plate in the specified frequency range.

Step 2. Use the data analysis system to obtain the natural frequencies from the frequency response data acquired in *Step 1*.

Step 3. Perform a narrow-band slow frequency sweep test near the natural frequency, allowing the fine sand on the plate to concentrate in areas with relatively small amplitude and visualize the mode shapes.

The frequency response data acquired from the test were drawn in the semi-logarithmic coordinate system (Figure 4), and the natural frequencies and the corresponding mode shapes are listed in Table 2.

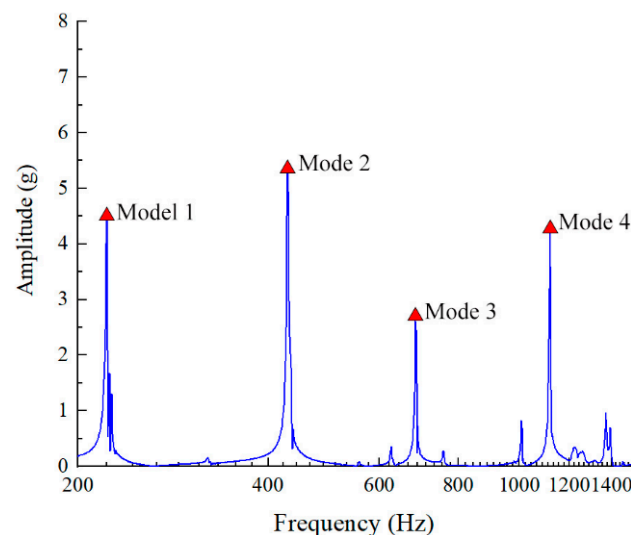
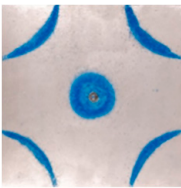
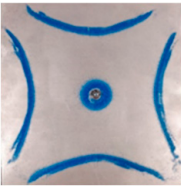
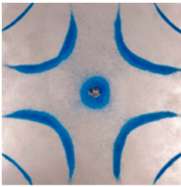
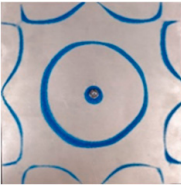


Figure 4. Frequency response curve of the plate under an acceleration excitation of 0.1 g.

Table 2. Experimental natural frequencies and mode shapes.

Mode	Frequency (Hz)	Mode Shape
1	221.44	
2	429.77	
3	684.89	
4	1117.92	

2.2. Finite Element Modal Analysis

First, a three-dimensional model of the plate was built (Figure 5). The reference material parameters and design dimensions of the plate are listed in Table 3. To automate the model-updating process, the FE model was parameterized, i.e., the material parameters and plate dimensions (including the length and thickness) were selected as the design variables. In addition, the constraint condition of the structure is another important factor affecting the FE modal-analysis results; thus, it needs to be taken into account. In this study, the constraint state of the bolted joint was simplified into two cases: perfect rigid constraint and elastic support constraint. The FE modal analysis with the perfect rigid constraint was performed first and the first 40 natural frequencies and displacement mode shapes of the plate are depicted in Figure 6. The red triangles in Figure 6 indicate the FE modes corresponding to the experimental modes, while the natural frequency errors between the experimental and FE modal-analysis results are listed in Table 4.

Table 3. Reference material parameters and design dimensions.

Type	Symbol	Item	Value
Material parameters	E	Young's modulus (GPa)	70.0
	μ	Poisson's ratio	0.33
	ρ	Density (kg/m^3)	2720
Design dimensions	L	Length (mm)	300
	T	Thickness (mm)	2
	D	Center hole diameter (mm)	9

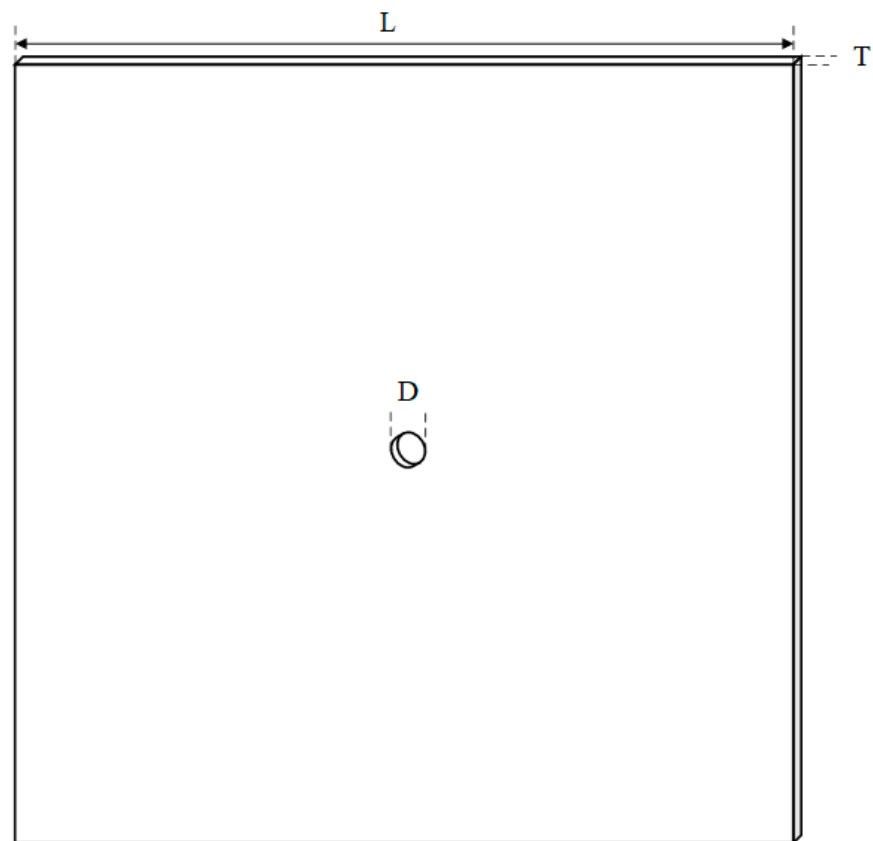


Figure 5. Three-dimensional model of the plate with dimensions.

Table 4. Natural frequency errors between the experimental and FE modal-analysis results.

Experimental Mode	Frequency (Hz)	FE Mode	Frequency (Hz)	Relative Error (%)
1	221.4	9	254.3	+14.82
2	429.8	14	489.9	+14.00
3	684.9	20	786.0	+14.76
4	1117.9	29	1270.4	+13.64

According to the results, there was a significant difference in the dynamic characteristics between the initial FE model and the actual structure; therefore, the FE model needs to be updated. In addition, the modes obtained by FE modal analysis were more than those measured in the experimental modal analysis. This difference is related to the direction and position of the excitation force. In the experimental modal analysis, the direction of the excitation force was unidirectional; thus, only the mode in that direction could be excited. On the other hand, in the FE modal analysis, modes in all directions can be easily obtained. Moreover, when the position of the excitation force is just near the node of the mode shape, where the vibration amplitude is close to zero, the mode will not be excited successfully. For instance, the FE mode shapes not measured in the experimental modal analysis have one thing in common; that is, the excitation position was in the low amplitude region (blue area in Figure 6) over the entire surface of the plate. Mode identification or mode-tracking techniques can effectively solve this problem of mode mismatch between experimental and FE modal-analysis results. Consequently, the research on a model-updating method with mode identification is worthy of attention.

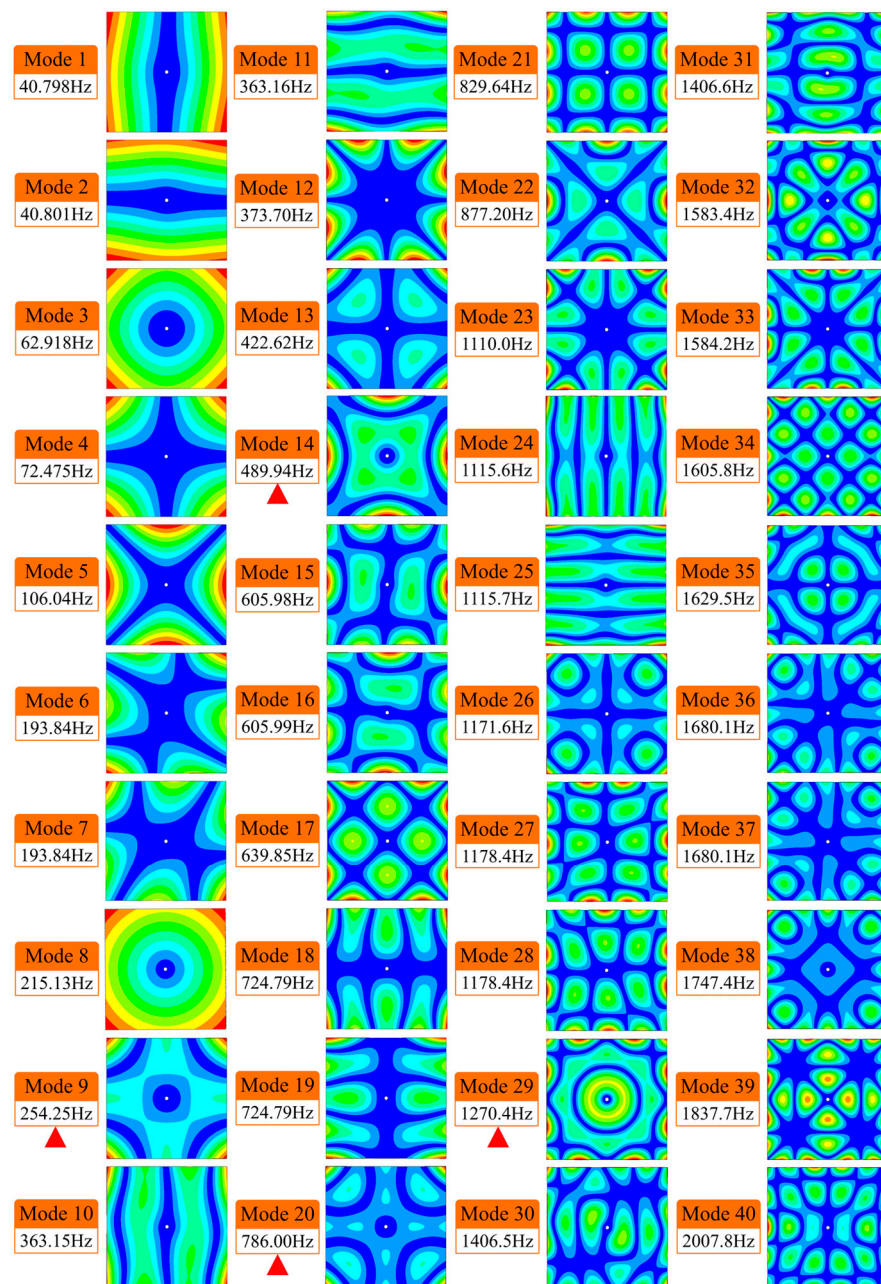


Figure 6. Natural frequencies and displacement mode shapes obtained by FE modal analysis.

3. Model-Updating with Automatic Mode Identification

3.1. Mode Identification Using Image-Similarity Recognition

In this study, the rough outline of the experimental mode shape was revealed by the accumulation of fine sand towards the low-amplitude region, which resulted in an inability to obtain accurate displacement information of the mode shape. Nevertheless, the corresponding relationship between the FE and experimental mode shapes can still be distinguished by comparing the mode shape patterns, which facilitates the mode identification using the image-similarity-recognition method. Considering that the FE mode shape contains richer information than the experimental one, it is difficult to directly calculate the similarity between them; thus, it is necessary to unify the mode shape for similarity recognition. The image unification process is depicted in Figure 7. During this process, a displacement threshold is set to extract the low-amplitude region of FE mode shape, and then, median filtering is applied to remove the noise from the experimental mode-shape image.

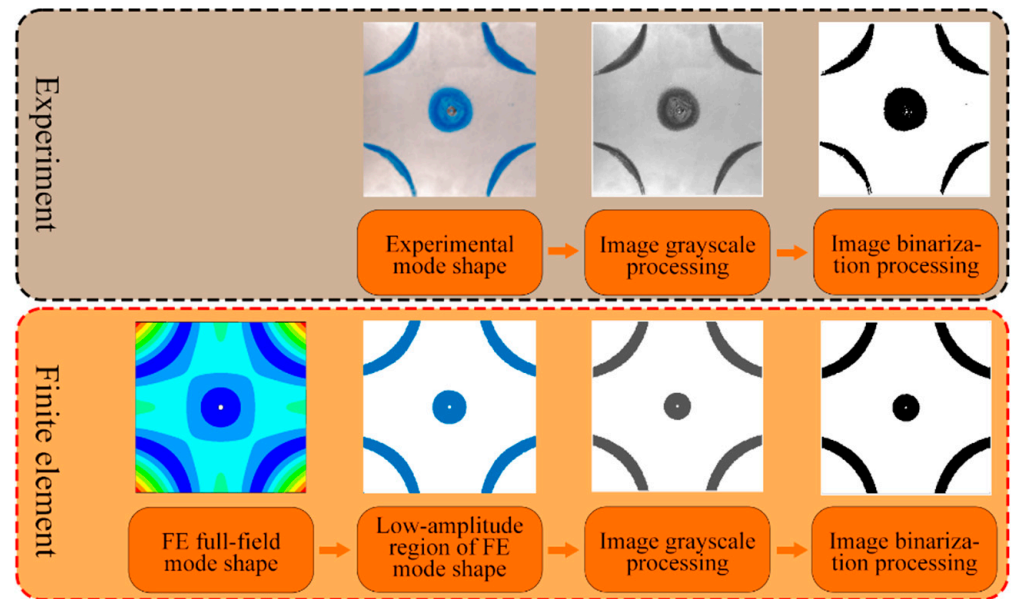


Figure 7. Image unification process of the FE and experimental mode shapes.

After unifying the mode shapes, the binarized images of the FE and experimental mode shapes are obtained. In a broad sense, the binarized image can be regarded as a binarization matrix. Therefore, the image-similarity-recognition problem is transformed into a matrix-similarity-recognition problem. Moreover, since the binarization matrix is composed only of 0 and 1, the effect of the element points in the image on the similarity recognition result is weakened, and the shape of the pattern in the image becomes the main factor that determines the similarity-recognition accuracy. The calculation process of the mode-identification index ISR refers to the MAC equation (proposed by Allemang [19]). First, the binarization matrices of the FE and experimental mode shapes are tiled into a vector form. Subsequently, the ISR can be calculated according to the following expression:

$$ISR(\Psi_R, \Psi_S) = \frac{(\Psi_R^T \Psi_S)^2}{(\Psi_S^T \Psi_S)(\Psi_R^T \Psi_R)} \tag{1}$$

where Ψ_R and Ψ_S are vectors of the reference and identified mode shapes, respectively. The obtained ISR is a scalar ranging from 0 to 1, and the higher its value, the higher the similarity.

To verify the validity and accuracy of mode identification using the ISR method, the first 40 mode shapes were extracted from the FE modal analysis and auto-correlation of these mode shapes was performed using the ISR index (Figure 8a). At the same time, the displacement mode shapes were extracted and the same calculation process was followed using the MAC proposed by Allemang (Figure 8b).

According to Figure 8, the colors on the diagonal are all red, indicating that the mode shapes to be identified are the same, and both indices achieved accurate mode identification. However, as shown in Figure 8b, many colors that are not on the diagonal are close to red, indicating that misjudgment is likely to occur when the MAC index is used to identify different mode shapes, while the ISR index can effectively avoid this problem (as shown in Figure 8a, most colors not on the diagonal are closer to blue). Thus, it can be concluded that ISR has higher sensitivity to the difference of mode shapes than MAC.

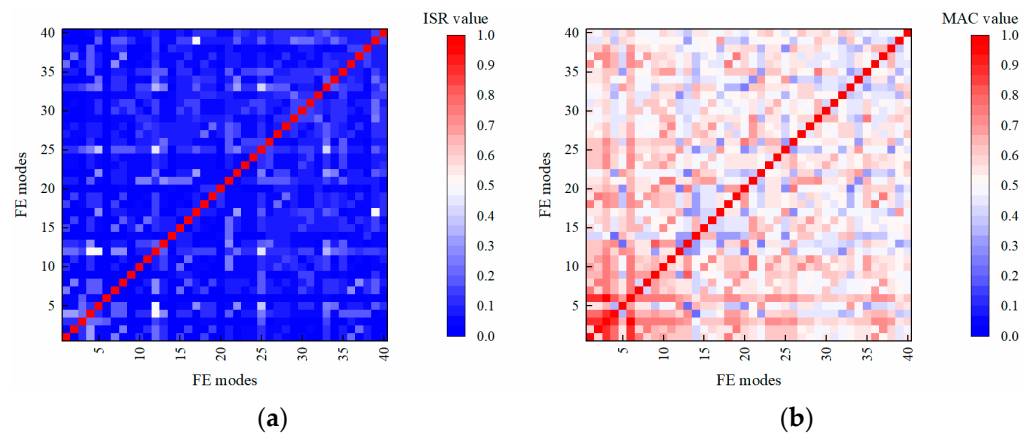


Figure 8. Auto-correlation of FE mode shapes based on different mode-identification indices (the closer the color is to red, the higher the similarity is, while the closer the color is to blue, the lower the similarity is). **(a)** Auto-correlation of FE mode shapes based on ISR and **(b)** Auto-correlation of FE mode shapes based on MAC.

3.2. Model-Updating Approaches

The model-updating method with automatic mode identification proposed in this paper comprises three modules: the modal-analysis module, the mode-identification module, and the model-updating module. In the modal-analysis module, the FE and experimental modal analyses are conducted separately to obtain the mode shapes and natural frequencies of the structure. In the mode-identification module, the similarity between the FE and experimental mode shapes is calculated using the ISR method, and the FE mode shape corresponding to the maximum ISR value is regarded as the same order mode as that of the experimental mode shape. The model-updating module, which includes the optimization algorithm and the parameterized FE model, is the key to driving the automatic execution of the model-updating process. A flow diagram of the model-updating method with automatic mode identification is illustrated in Figure 9.

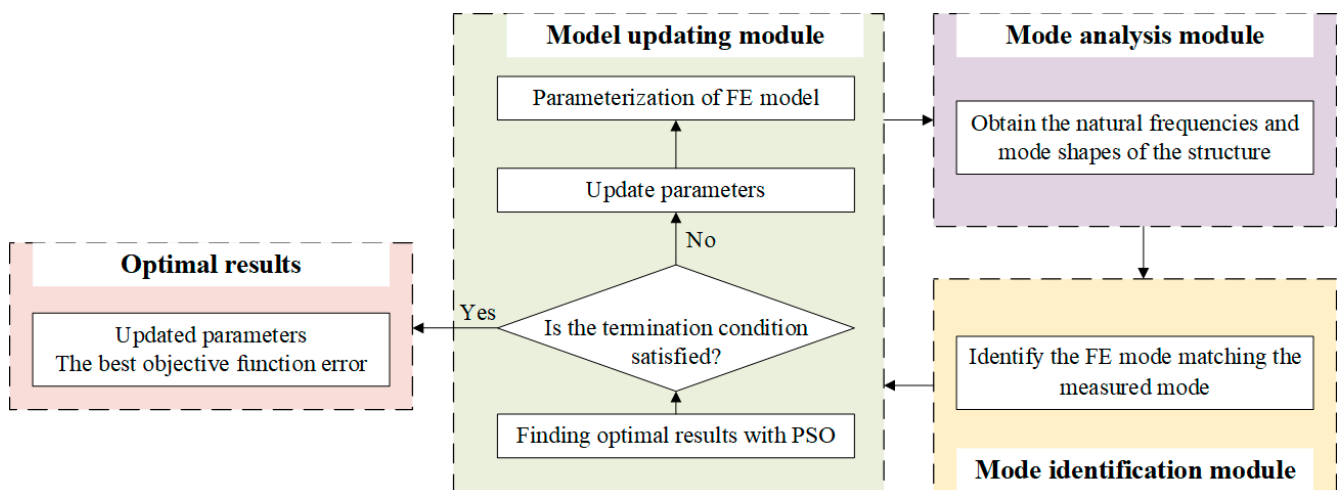


Figure 9. Flow diagram of the model-updating method with automatic mode identification.

This study focuses on the impact of the boundary constraints on model-updating. To properly represent the boundary constraints, two different model-updating approaches are proposed and followed, as described in Table 5. The updating variables used in each approach are related to the boundary conditions, material properties, and structure dimensions.

Table 5. Updating variables for the different model-updating approaches.

	First Approach	Second Approach
Updating variables	Perfect rigid constraint	k_H k_V
	Young’s modulus	Young’s modulus
	Poisson’s ratio	Poisson’s ratio
	Density	Density
	Length	Length
	Thickness	Thickness

In the first approach, the boundary constraint is regarded as perfect rigid constraint; that is, the accuracy of model-updating is related only to the material properties and dimensions. In the second approach, an elastic support constraint is assumed, and the contact surface of the components is simplified to a number of springs in order to quantitatively characterize the support stiffness. In this paper, the plate was fixed to the exciter by a bolt, and the contact surface was the inner surface of the circular hole at the center of the plate. During model constraint simplification, the contact surface was discretized, and three springs in orthogonal directions were used on each node to simulate the elastic support between bolt and hole wall (Figure 10). The springs parallel to the surface of the plate provided support in the x- and y-directions. Since the support in these two directions is generated by the friction and extrusion between the components, k_H was used to characterize the stiffness of the springs in these two directions. The springs on the vertical surface of the plate provided support in the z-direction. The support in this direction is mainly caused by the extrusion of the components; thus, k_V was used to represent the stiffness of the z-direction springs.

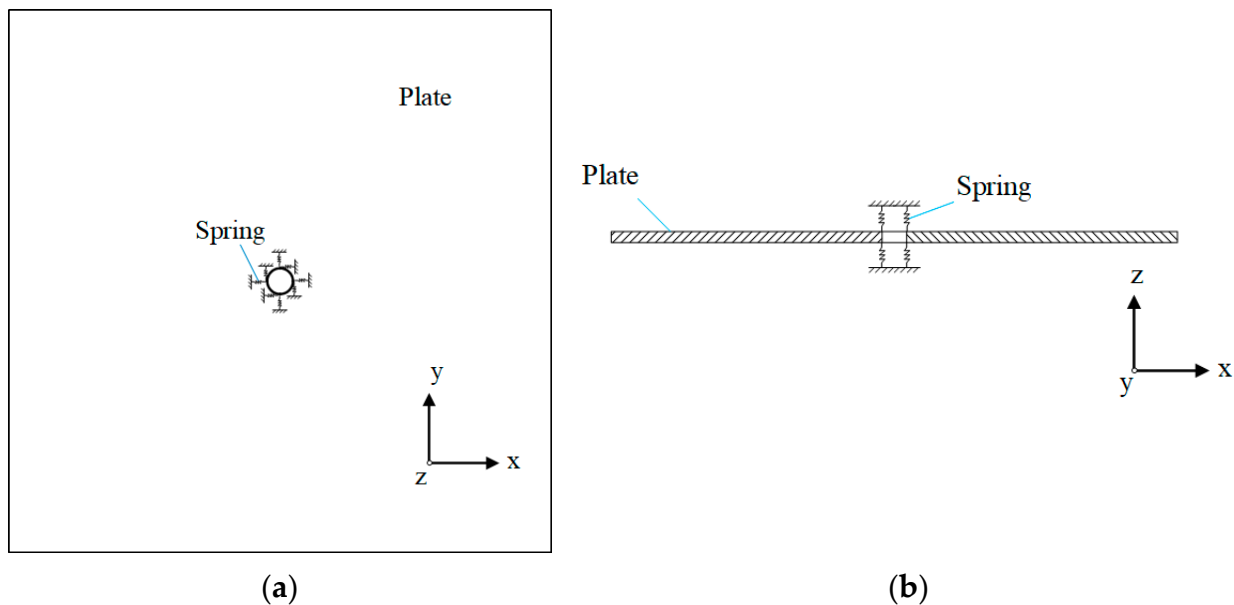


Figure 10. Schematic diagrams of the support springs. (a) x- and y-direction springs and (b) z-direction springs.

4. Optimization

4.1. Particle Swarm Optimization

In this study, the PSO method is employed to find the optimal updating parameters for constructing an accurate FE model. The optimization steps are as follows:

Step 1. Randomly initialize the velocity and position of each particle.

Step 2. Evaluate the fitness of each particle; record the best position of each particle p_{best} and the best global position g_{best} .

Step 3. Determine whether the conditions for the end of the iteration are met; if yes, terminate the calculation and output the optimal result; otherwise, continue to the following step.

Step 4. Update the velocity and position of each particle according to Equation (2) and Equation (3), and return to Step 2.

$$v_i(t + 1) = \omega v_i(t) + c_1 r_1 (p_{\text{best}}(t) - x_i(t)) + c_2 r_2 (g_{\text{best}}(t) - x_i(t)) \quad i = 1, 2, \dots, N \quad (2)$$

$$x_i(t + 1) = x_i(t) + v_i(t + 1) \quad (3)$$

where i is the particle number, N is the total number of particles, t is the t – th iteration, ω is the inertia weight, r_1 and r_2 are random values from 0 to 1, and c_1 and c_2 denote the self-learning factor of the particles and the group learning factor, respectively. Before using the PSO method for model-updating, the parameters in the PSO algorithm are set as presented in Table 6. In this method, the larger the number of particles, the easier it is to find the optimal value in the full design domain, but the higher the time consumption. In this work, N was set to 20, 30, and 50 to find a balance between calculation cost and accuracy of the result. In addition, in order to ensure the full convergence of the process of finding the optimal value, the maximum number of iterations $t_{\text{max}} = 20$ was set as the termination condition.

Table 6. Parameter setting in the PSO algorithm.

Parameter	N	ω	c_1	c_2	t_{max}
Value	20, 30, 50	0.8	2	2	20

4.2. Updating Parameter Limits and Objective Function

As an important part of the optimization process, the limits of the updating parameters need to be carefully defined [24]. The present work includes up to seven updating parameters, which can be divided into three groups: support stiffness, material properties, and structure dimensions.

The material of the plate was aluminum–magnesium (Al–Mg) alloy, and the material properties, including the Young’s modulus, Poisson’s ratio, and density, were selected as updating parameters. Normally, these properties are set as constants; however, differences in the material composition and its manufacturing process can induce certain variations. The limits for these parameters were determined by an analogue approach. The material properties of several typical Al–Mg alloys are listed in Table 7. The maximum and minimum values of each material parameter were used as the upper and lower limits of the updating parameters, respectively.

Table 7. Material properties of several typical Al–Mg alloys [25].

Material Type	Young’s Modulus (GPa)	Poisson’s Ratio	Density (kg/m ³)
5042	68.9	0.33	2720
5052	72	0.34	2680
5052-H34	70	0.33	2680
5083-H116	70	0.3	2700
5182	76	0.34	2720
5182-O	70.6	0.34	2890
Upper limit	76	0.34	2890
Lower limit	68.9	0.3	2680

The two actual dimensions of the plate, i.e., length and thickness, deviated from the design dimensions, and there was also a deviation in the dimensions measured at different positions. Therefore, the measured dimensions cannot be used directly to build

the FE model. In order to determine the limits of the dimensions, it was assumed that the dimensions measured at different positions conform to the normal distribution, and a 95.45% confidence level was chosen, as described in the following relationship:

$$P(\mu - 2\sigma \leq X \leq \mu + 2\sigma) \approx 0.9545 \tag{4}$$

where X is a random variable, μ is the mean value, and σ is the standard deviation. In this work, μ and σ were calculated from the measurements. The limits for the length and thickness of the plate were set to be the mean value of the measurements with a deviation of $+2\sigma$ for the upper limits and -2σ for the lower limits. The optimal dimensions have a 95.45% chance of being inside the given interval.

Finally, the limits of the stiffness of the springs used to simulate the support stiffness in the horizontal (k_H) and vertical (k_V) directions were defined. Before determining the limits, the sources of the support stiffness in both directions were analyzed. In the vertical direction (k_V), the support stiffness of the plate mainly comes from the extrusion between the components, which is in accordance with Hooke’s law:

$$F = EA\varepsilon \tag{5}$$

where F is the support force, E is the Young’s modulus of the plate, A is the contact area between plate and exciter, ε is the strain, and EA is the stiffness of the system. When A takes the maximum value of 250.5 mm^2 , EA can be used as the upper limit of k_V . Considering that the elastic deformation is not the only reason for the support stiffness in this direction, this upper limit can be taken as a higher value. In the horizontal direction (k_H), the support stiffness mainly comes from the friction between the components. Since the friction contact surface is the same as the extrusion contact surface mentioned above, the friction coefficient can be introduced into Equation (5), and the relationship between deformation and friction force can take the following form:

$$F = \mu EA\varepsilon \tag{6}$$

where μ is the friction coefficient and its value is about 0.1. As a result, the upper limit of k_H can be determined by the upper limit of k_V . Due to the lack of sufficient theoretical basis, the lower limits cannot be set accurately; thus, the lower limits of k_H and k_V were taken as a smaller value relative to the value of their respective upper limits. The lower and upper limits of all updating parameters are listed in Table 8.

Table 8. Updating parameter limits.

Updating Parameters	Lower Limit	Upper Limit
k_H (N/m)	10^4	10^8
k_V (N/m)	10^5	10^9
Young’s modulus (GPa)	68.9	76
Poisson’s ratio	0.3	0.34
Density (kg/m^3)	2680	2890
Length (mm)	296.81	303.10
Thickness (mm)	1.89	2.11

In this work, the four-order natural frequencies obtained experimentally and those obtained numerically were used to construct the following objective function:

$$F_{\text{obj}} = \sqrt{\frac{\sum_{i=1}^4 \omega_i \left(\frac{f_i^{\text{exp}} - f_i^{\text{num}}}{f_i^{\text{exp}}} \right)^2}{\sum_{i=1}^4 \omega_i}} \tag{7}$$

where ω_i is the weight coefficient of the natural frequency error of each order, f_i^{exp} is the i -th order experimental natural frequency, and f_i^{num} is the numerical natural frequency

corresponding to f_i^{exp} . Through this objective function, by increasing the value of ω_i , the i -th order experimental natural frequency error is easier to obtain a smaller value. In this work, ω_i was set to the same value.

The optimization model of the second model-updating approach can be expressed by Equation (8).

$$\begin{aligned}
 \text{Minimize } F_{obj} &= \sqrt{\frac{\sum_{i=1}^4 \omega_i \left(\frac{f_i^{exp} - f_i^{num}}{f_i^{exp}} \right)^2}{\sum_{i=1}^4 \omega_i}} \\
 \text{S.T. } &k_H \leq k_H \leq \bar{k}_H \\
 &k_V \leq k_V \leq \bar{k}_V \\
 &\underline{E} \leq E \leq \bar{E} \\
 &\underline{\mu} \leq \mu \leq \bar{\mu} \\
 &\underline{\rho} \leq \rho \leq \bar{\rho} \\
 &\underline{L} \leq L \leq \bar{L} \\
 &\underline{T} \leq T \leq \bar{T}
 \end{aligned} \tag{8}$$

In this equation, the objective function is minimized, and the limits to which the problem is subject (S.T.), consisting of the lower and upper limits of the updating parameters.

4.3. Mode Switching Order Range Estimation Using Latin Hypercube Sampling

In the proposed method, the mode-identification process consumes most of the computational time. To improve the efficiency of mode identification and reduce the time cost, it is necessary to avoid the identification of all modes one-by-one. Therefore, Latin hypercube sampling (LHS) was employed to perform probability statistics of the switching range of the concerned modes, and the mode orders to be identified were reduced according to the statistical results.

LHS is an approximate random sampling method from multivariate parameter distribution, which was first proposed by McKay [26]. The samples generated by LHS are distributed evenly in the variable domain, and the objective domain of these samples has a high similarity to the actual objective domain. Thus, the statistical results of LHS can represent the actual results with high credibility. For the model-updating approaches proposed in this work, the distribution of LHS samples in the design variables space and the switching range of the concerned mode orders are presented in Figures 11 and 12, respectively.

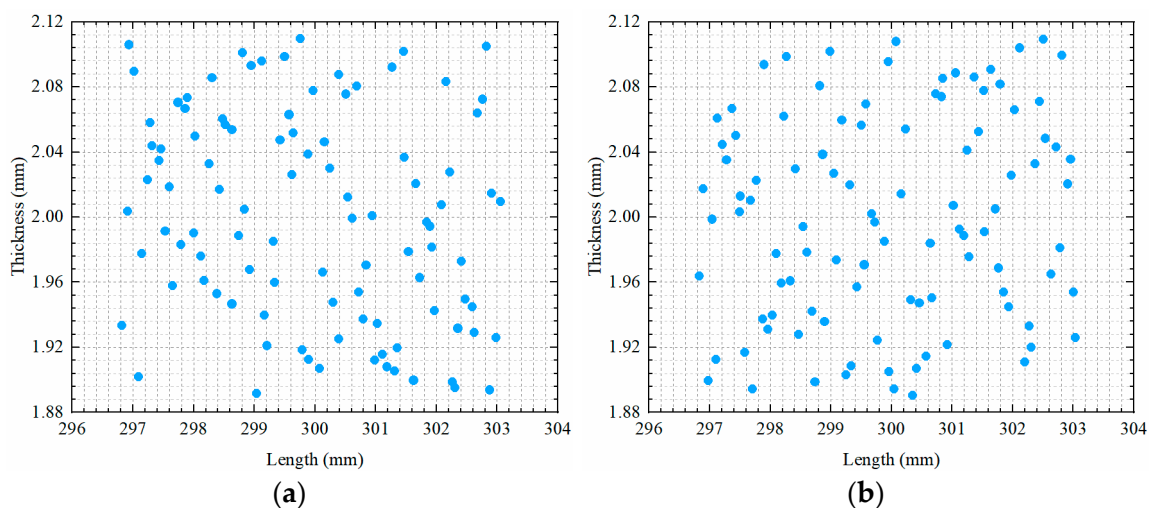


Figure 11. Distribution of LHS samples. (a) First model-updating approach and (b) second model-updating approach.

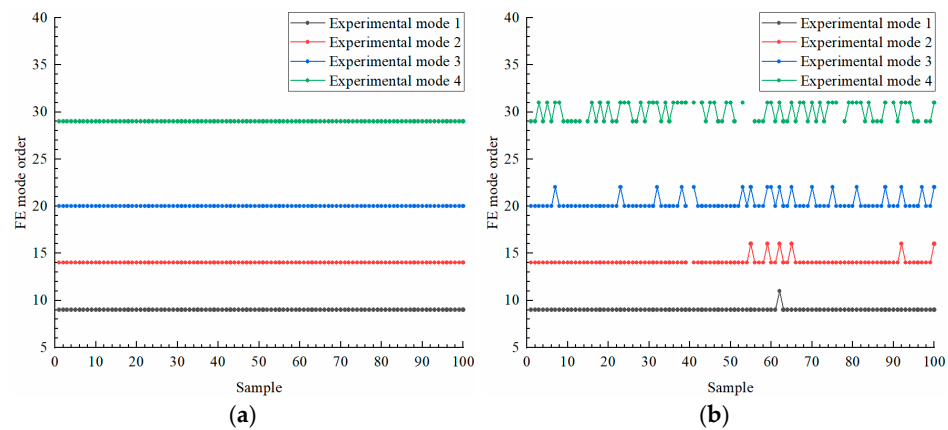


Figure 12. Switching range of the concerned mode orders. (a) First model-updating approach and (b) second model-updating approach.

Based on the above statistical results, the mode orders to be tracked in the two model-updating approaches were determined, as shown in Table 9.

Table 9. Mode orders to be tracked in the two model-updating approaches.

Experimental Mode Order	First Approach FE Mode Order	Second Approach FE Mode Order
1	9	9, 11
2	14	14, 16
3	20	20, 22
4	29	29, 31

5. Results and Discussion

5.1. Convergence of the PSO Simulations and Mode Tracking

As presented in Table 6, both approaches were performed using three different numbers of particles. The minimum objective function errors and calculation time of these simulations are listed in Table 10. It can be observed that the smallest error was obtained with the second approach, and overall, the errors of the second approach were better than those of the first one. Consequently, the assumption of using springs to simulate the constraint support stiffness is valid. In addition, based on the results, it can also be concluded that the increase of the number of particles inevitably leads to a significant increase in the calculation time, while the optimization results are not improved significantly. Thus, it is necessary to find a fine balance between calculation time and accuracy of the results.

Table 10. Minimum objective function errors and calculation time of the PSO simulations.

Number of Particles	First Approach		Second Approach	
	Error (%)	Time (h)	Error (%)	Time (h)
20	2.78	13.42	1.14	12.75
30	1.40	21.60	1.05	19.13
50	1.40	33.34	1.07	24.73

Figure 13 displays the convergence plots of the PSO simulations with different numbers of particles. Based on the results, the convergence of the PSO simulations can be divided into two stages: the fast convergence stage and the stable convergence stage. In the first stage, the fitness values of the particles are relatively scattered, while the mean value of the particle swarm and the minimum error converge rapidly. In the second stage, the particle swarm tends to concentrate towards the minimum error and their mean value decreases slowly. Furthermore, the increase in the number of particles does not significantly affect the convergence rate of the PSO simulation, but only increases the probability of the

particle swarm finding the optimal value. This is also one of the reasons why the accuracy of the results does not necessarily improve with the increase of the number of particles. From the results listed in Table 10, setting the number of particles to 30 is recommended in this work.

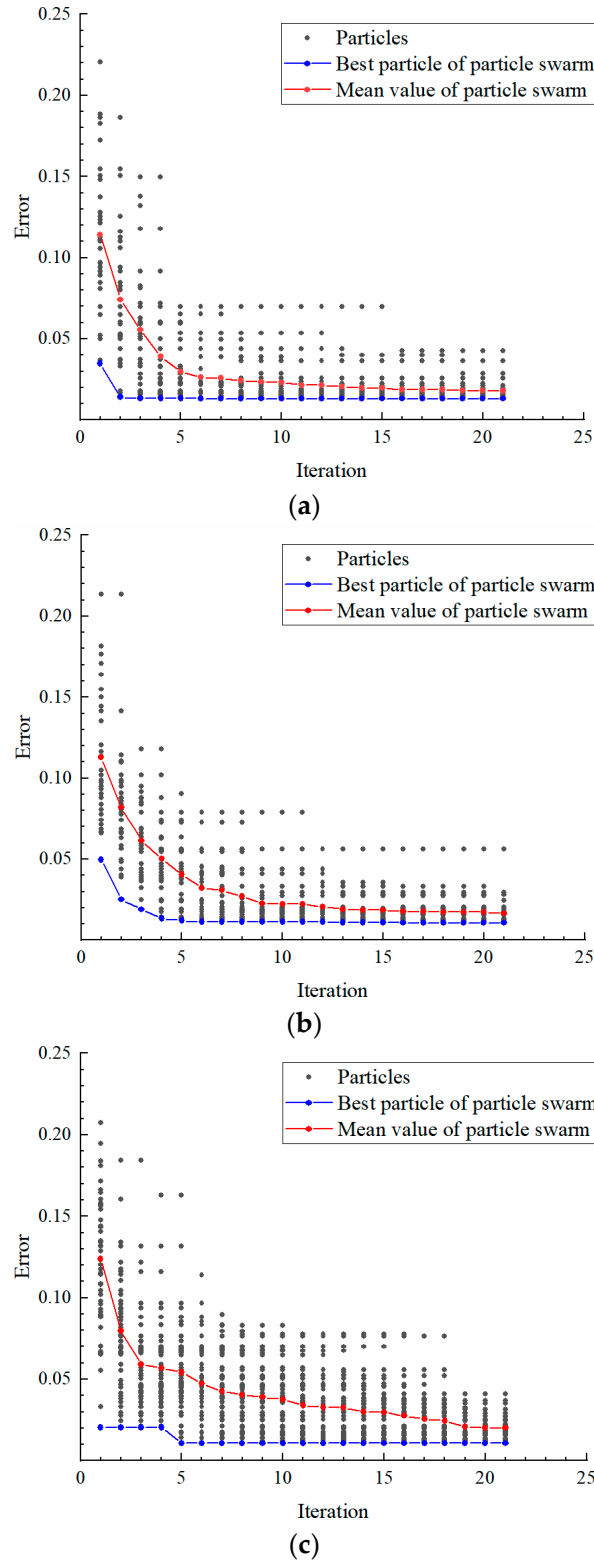


Figure 13. Convergence plots of the PSO simulations for the second approach using different numbers of particles. (a) 20 particles, (b) 30 particles, and (c) 50 particles.

During the process of optimization iteration, the mode-tracking results of a particle using the ISR index in the first and second approaches are presented in Figure 14. It can be observed that the ISR index could effectively identify the modes, and the order of the modes to be identified was within the previously-determined mode switching range. Moreover, the probability of mode switching in the second approach was higher than in the first approach, which leads to the conclusion that the constraint state is an important factor affecting the order of modes.

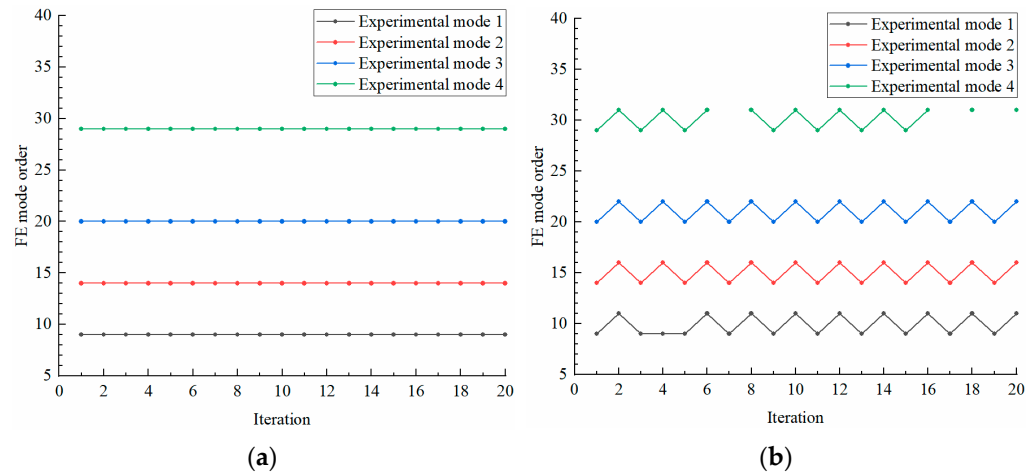


Figure 14. Mode tracking for the first and second approaches. (a) Mode tracking for the first approach and (b) mode tracking for the second approach.

5.2. Results with Different Model-Updating Approaches

The optimal results, including the minimum errors of the objective function and the natural frequencies, for the two approaches and the updated parameters are listed in Table 11. The objective function error of the original FE model, which was constructed according to the reference parameters in Table 3, was as high as 14.31%. The errors of the models updated by the first and second approaches were reduced to 1.40% and 1.05%, respectively. Since the weight coefficients of the four-order frequency errors were the same, the error gap was small. For the second approach, the maximum and minimum errors were 1.46% and 0.44%, respectively.

Table 11. Optimal results and updated parameters.

	Experiment	Original FE Model	First Approach	Second Approach
k_H (N/m)		∞	∞	10^8
k_V (N/m)		∞	∞	10^9
Young's modulus (GPa)	-	70.0	68.9	69.1
Poisson's ratio		0.33	0.3	0.3
Density (kg/m^3)		2720	2890	2890
Length (mm)		300	303.1	302.9
Thickness (mm)		2	1.89	1.89
F_{obj} (%)		14.31	1.40	1.05
First natural frequency (Hz)	221.4	254.3	226.0 (+2.06%)	223.5 (+0.93%)
Second natural frequency (Hz)	429.8	489.9	434.4 (+1.08%)	427.9 (-0.44%)
Third natural frequency (Hz)	684.9	786.0	694.9 (+1.46%)	692.5 (+1.11%)
Fourth natural frequency (Hz)	1117.9	1270.4	1124.6 (+0.60%)	1101.6 (-1.46%)

5.3. Application and Limitation

The method proposed in this paper is not applicable to plate structures or to other types of structures. In practical applications, how to obtain accurate modal pairs (frequencies and mode shapes) information of the structure is the primary problem to be solved. Regarding frequency measurement, it should be noted that the installation position of the sensor should not be arranged at the mode-shape node line, and the installation direction should be consistent with the excitation direction. In addition, if the mass of the structure to be measured is small, non-contact measurement is recommended. Regarding mode-shape measurement, the measurement method used in this paper is suitable for plate structures, and for non-plate structures, it can be obtained by rationally arranging multiple measurement sensors or using advanced scanning laser vibrometers. Building an optimization model for model-updating is another key step in the proposed method. In this step, it is necessary to select reasonable correction parameters according to the actual situation, and determine the value range of each parameter. Furthermore, this paper simplifies the boundary constraints into a series of springs, which can provide a solution for the quantitative characterization of complex boundary constraints in the FE modeling process.

Nevertheless, this method still has certain limitations. Although LHS was used to count the mode-switching range, thereby reducing the identification orders, the calculation time remained as high as 33.34 h. This was due to the need to call the FE software to re-perform modal analysis of the FE model for each calculation. In future work, in order to further reduce the calculation time, it is necessary to introduce an approximate model instead of the FE model for modal analysis. Moreover, for complex engineering structures, it is often difficult to measure the mode shape. When the measured mode shapes are distorted or unavailable, this method will fail.

6. Conclusions

In this paper, a mode-identification index based on image-similarity recognition was proposed to identify the analytical modes matching the measured modes. In addition, a structural dynamic model-updating method with automatic mode identification using particle swarm optimization was developed to obtain a high-precision FE model. Subsequently, a parameterized FE model of a square plate was built and updated by using the proposed model-updating method. Two different model-updating approaches were investigated in this work. In the first approach, the connection condition was regarded as perfect rigid constraint; that is, the support stiffness of the connecting interface was infinite. In the second approach, the connection condition was simplified by a series of springs. To reduce the computational time, probability statistics of the mode-switching range were performed using LHS, and the results revealed that the modes concerned will only be switched within the range of adjacent orders; this indicated that it is not necessary to identify all modes one-by-one. Finally, two model-updating approaches were followed using three different numbers of particles. The results indicated that both approaches can successfully obtain a high-precision FE model, and the second approach produced the smallest objective function error. It can also be concluded that the model-updating accuracy can be improved by simplifying the boundary conditions as a series of springs, which can be used as updating parameters.

Author Contributions: Conceptualization, J.F. and B.S.; methodology, K.L.; validation, K.L. and Y.L.; formal analysis, K.L.; investigation, K.L.; resources, B.S. and J.F.; data curation, K.L.; writing—original draft preparation, K.L.; writing—review and editing, J.F.; visualization, K.L.; supervision, J.F.; project administration, G.C.; funding acquisition, J.F. All authors have read and agreed to the published version of the manuscript.

Funding: This research was funded by the National Natural Science Foundation of China (Grant No. 51306007).

Institutional Review Board Statement: Not applicable.

Informed Consent Statement: Not applicable.

Data Availability Statement: Not applicable.

Conflicts of Interest: The authors declare no conflict of interest.

References

1. Mottershead, J.E.; Friswell, M.I. Model updating in structural dynamics: A survey. *J. Sound Vib.* **1993**, *167*, 347–375. [\[CrossRef\]](#)
2. Bagha, A.K.; Gupta, P.; Panwar, V. Finite element model updating of a composite material beam using direct updating method. *Mater. Today Proc.* **2020**, *27*, 1947–1950. [\[CrossRef\]](#)
3. Liu, F.; Li, H.; Qin, H.; Liang, B. Added mass matrix estimation of beams partially immersed in water using measured dynamic responses. *J. Sound Vib.* **2014**, *333*, 5004–5017. [\[CrossRef\]](#)
4. Hu, S.L.J.; Li, H.; Wang, S. Cross-model cross-mode method for model updating. *Mech. Syst. Signal Process.* **2007**, *21*, 1690–1703. [\[CrossRef\]](#)
5. Li, Y.; Tian, K.; Hao, P.; Wang, B.; Wu, H.; Wang, B. Finite element model updating for repeated eigenvalue structures via the reduced-order model using incomplete measured modes. *Mech. Syst. Signal Process.* **2020**, *142*, 106748. [\[CrossRef\]](#)
6. Wu, W.H.; Prendergast, L.J.; Gavin, K. An iterative method to infer distributed mass and stiffness profiles for use in reference dynamic beam-Winkler models of foundation piles from frequency response functions. *J. Sound Vib.* **2018**, *431*, 1–19. [\[CrossRef\]](#)
7. Xu, H.; Qin, D.; Liu, C.; Zhang, Y. An Improved Dynamic Model Updating Method for Multistage Gearbox Based on Surrogate Model and Sensitivity Analysis. *IEEE Access* **2021**, *9*, 18527–18537. [\[CrossRef\]](#)
8. Simoen, E.; De, R.G.; Lombaert, G. Dealing with uncertainty in model updating for damage assessment: A review. *Mech. Syst. Signal Process.* **2015**, *56*, 123–149. [\[CrossRef\]](#)
9. Lin, R.M.; Zhu, J. Model updating of damped structures using FRF data. *Mech. Syst. Signal Process.* **2006**, *20*, 2200–2218. [\[CrossRef\]](#)
10. Esfandiari, A.; Sanayei, M. More insight on function-weighted frequency response function sensitivity method for analytical model updating. *J. Sound Vib.* **2021**, *509*, 116143. [\[CrossRef\]](#)
11. Zin, M.S.M.; Rani, M.N.A.; Yunus, M.A.; Mirza, W.I.I.W.I. Frequency Response Function Based Updating of a Laser Spot Welded Structure using Synthesised Frequency Response Function. *IOP Conf. Ser. Mater. Sci. Eng.* **2019**, *506*, 012012.
12. Saeed, Z.; Firrone, C.M.; Berruti, T.M. Hybrid Numerical-Experimental Model Update Based on Correlation Approach for Turbine Components. *J. Eng. Gas Turbines Power* **2021**, *143*, 041009. [\[CrossRef\]](#)
13. Guo, N.; Yang, Z.; Wang, L.; Ouyang, Y.; Zhang, X. Dynamic model updating based on strain mode shape and natural frequency using hybrid pattern search technique. *J. Sound Vib.* **2018**, *422*, 112–130. [\[CrossRef\]](#)
14. Nehete, D.V.; Modak, S.V.; Gupta, K. Experimental studies in finite element model updating of vibro-acoustic cavities using coupled modal data and FRFs. *Appl. Acoust.* **2019**, *150*, 113–123. [\[CrossRef\]](#)
15. Das, A.; Debnath, N. A Bayesian model updating with incomplete complex modal data. *Mech. Syst. Signal Process.* **2020**, *136*, 106524. [\[CrossRef\]](#)
16. Lin, R.M.; Ewins, D.J. Model updating using FRF data. In Proceedings of the 15th International Modal Analysis Seminar, Leuven, Belgium, 17–21 September 1990; pp. 141–163.
17. Lin, R.M.; Ewins, D.J. Analytical model improvement using frequency response functions. *Mech. Syst. Signal Process.* **1994**, *8*, 437–458. [\[CrossRef\]](#)
18. Chen, S.; Zheng, Y.; Liu, Y. Structural optimization with an automatic mode identification method for tracking the local vibration mode. *Eng. Optim.* **2018**, *50*, 1681–1694. [\[CrossRef\]](#)
19. Allemang, R.J. A correlation coefficient for modal vector analysis. In Proceedings of the 1st International Modal Analysis Conference, Orlando, FL, USA, 8–10 November 1982; pp. 110–116.
20. Ngan, J.W.; Caprani, C.C.; Bai, Y. Full-field finite element model updating using Zernike moment descriptors for structures exhibiting localized mode shapes. *Mech. Syst. Signal Process.* **2019**, *121*, 373–388. [\[CrossRef\]](#)
21. Kennedy, J.; Eberhart, R. Particle swarm optimization. In Proceedings of the ICNN'95—International Conference on Neural Networks, Perth, WA, Australia, 27 November 1995–1 December 1995; Volume 4, pp. 1942–1948.
22. Dilek, A.U.; Oguz, A.D.; Satis, F.; Gokdel, Y.D.; Ozbek, M. Condition monitoring of wind turbine blades and tower via an automated laser scanning system. *Eng. Struct.* **2019**, *189*, 25–34. [\[CrossRef\]](#)
23. Silva, A.C.S.; Sebastian, C.M.; Lambros, J.; Patterson, E.A. High temperature modal analysis of a non-uniformly heated rectangular plate: Experiments and simulations. *J. Sound Vib.* **2019**, *443*, 397–410. [\[CrossRef\]](#)
24. Negri, D.; Fiorentin, F.K.; Filho, J.M.C. A model updating method for plate elements using particle swarm optimization (PSO), modeling the boundary flexibility, including uncertainties on material and dimensional properties. *Lat. Am. J. Solids Struct.* **2018**, *15*, 1–18. [\[CrossRef\]](#)
25. Xin, C.L. *FEA Common Material Parameter Manual*; China Machine Press: Beijing, China, 2019.
26. McKay, M.D.; Beckman, R.J.; Conover, W.J. A comparison of three methods for selecting values of input variables in the analysis of output from a computer code. *Technometrics* **2000**, *42*, 55–61. [\[CrossRef\]](#)